

## Quality open source mesh generation for biological flow simulations

E.Marchandise\*, E.Sauvage\*, and JF. Remacle\*

\* Université catholique de Louvain, institute of Mechanics,  
Materials and Civil Engineering (iMMC), Belgium  
emilie.marchandise@uclouvain.be, emilie.sauvage@uclouvain.be,  
jean-francois.remacle@uclouvain.be

### Abstract

We present efficient algorithms for generating quality tetrahedral meshes for biological flow simulations starting from low quality triangulations obtained from the segmentation of patient specific medical images. The suite of algorithms that are presented in this paper have been implemented in the open-source mesh generator Gmsh [8]. This includes a high quality remeshing algorithm based on a finite element discrete parametrization and a volume meshing algorithm with a boundary layer generation technique. In the result section, we show that the presence of a boundary layer mesh plays an important role to reduce the problem size in cardiovascular flow simulations.

**Keywords:** Surface meshing, remeshing, harmonic map, boundary layer, quality mesh, numerical simulation

### Introduction

In the biomedical field, the geometrical data acquired via medical imaging techniques (CT or MRI) is often a triangulation obtained directly from segmentation. This triangulation is generally oversampled, of very low quality and often with broken topology. Actually this is still a bottleneck in the domain of biomedical computation. Indeed creating high quality meshes is an essential feature for obtaining accurate and efficient numerical solutions of partial differential equations that model the physiological systems. Unfortunately, those STL surface meshes are generally of too low quality to be directly used for numerical simulations. While many commercial packages offer mesh generation options, these depend on high quality input, which is rarely available when depending on image segmentation results.

In this paper we first propose an efficient approach for recovering a high quality surface mesh from a low quality input (STL triangulation). The technique is based on discrete finite element maps [17] with appropriate boundary conditions. We discuss and compare two different types of harmonic mappings : the Laplacian harmonic map and the conformal map.

The proposed quality surface remeshing algorithm is of high importance for subsequent three-dimensional biological flow simulations. Indeed, the surface triangulation is most of the time taken as input for the tetrahedral mesh generator (e.g. Delaunay, Frontal), which retains the remeshed surface as the boundary of the resulting tetrahedral mesh. Hence if the surface mesh contains low quality triangles with small angles, the resulting tetrahedral mesh

might contain some degenerate tetrahedra with small volumes and small dihedral angles. Those degenerate triangles may lead to large interpolation errors, and have a negative effect on the convergence rate of the solution procedure. The worst impact results in an unresolvable system of equations.

In the context of biological flow simulations, another important point concerns the generation of a mesh boundary layer that is able to capture at the vicinity of the wall derived quantities of clinical interest. While many authors still use fully unstructured isotropic tetrahedral meshes, these meshes are not efficient in terms of computational time. Indeed, they require a huge number of elements in order to have sufficiently small elements near the wall to resolve the boundary layer and to be able to capture accurately derived quantities such as WSS. Moreover, some authors have reported that these meshes can produce spurious fluctuations for the WSS [19, 21]. Boundary layer meshes permit to capture those derived quantities accurately while keeping for efficiency purposes a reasonable number of mesh elements.

In the second part of this paper, we present an advancing layer method [6, 7, 9] that extrudes the lumen surface mesh in the inward direction. The extruded prisms are then subsequently split into tetrahedra and the remaining of the lumen volume filled with tetrahedra.

An example of blood flow simulation with a remeshed aortic arch is presented. The overall (re)meshing procedure is implemented in the open-source mesh generator Gmsh ([www.gmsh.geuz.org](http://www.gmsh.geuz.org)) [8].

## Surface meshes

The remeshing technique we present is based on a discrete parametrization of a given mesh patch  $S$  that is also called discrete surface. We first assume we have automatically split our initial triangulation into different mesh patches that satisfy the three following conditions: have zero genus, have a boundary that is made of at least one closed curve, have a moderate geometrical aspect ratio (see [12, 13] for more details). Next we compute for each patch a finite element harmonic map, and then remesh the patch in the parametric space using standard 2D mesh generators with a prescribed mesh size field. Figure 1 shows both an initial triangular mesh of  $S$  and its map onto the unit disk. The surface  $S$  results from the segmentation of an anastomosis site in the lower limbs, more precisely a bypass of an occluded femoral artery realized with the patient's saphenous vein. The unit disk contains two holes that correspond to the boundary of the femoral artery  $\partial S_2$  and the saphenous vein  $\partial S_3$  on which we have imposed Neumann boundary conditions.

Let us define now the discrete parametrization of a mesh patch  $S$  with a conformal map. Parametrizing such a patch  $S$  is defining a map  $\mathbf{u}(\mathbf{x})$  (see Fig. 1):

$$\mathbf{x} \in S \subset \mathbb{R}^3 \mapsto \mathbf{u}(\mathbf{x}) \in S' \subset \mathbb{R}^2 \quad (1)$$

that transforms continuously a 3D patch  $S$  into a patch  $S'$  embedded in  $\mathbb{R}^2$  that has a well known parametrization. Two type of mappings are implemented: a harmonic map and a least square conformal map.

A harmonic map minimizes distortion in the sense that it minimizes the Dirichlet energy of the mapping  $\mathbf{u}(\mathbf{x})$ :

$$E_D(\mathbf{u}) = \int_M \frac{1}{2} |\nabla \mathbf{u}|^2 ds. \quad (2)$$

subject to Dirichlet boundary conditions  $\mathbf{u} = \mathbf{u}_D$  on  $\partial M^i$ . Harmonic maps are not in general conformal and do not preserve angles but they are popular since they are very easy to compute and are guaranteed to be one-to-one for convex regions [3, 16].

The least square conformal map as introduced by Levy et al. [11] asks that the gradient of  $u$  and the gradient of  $v$  shall be as orthogonal as possible in the parametrization and have the same norm. This can be seen as an approximation of the Cauchy-Riemann equations. For a piecewise linear mapping, the least square conformal map can be obtained by minimizing the conformal energy:

$$E_{\text{LSCM}}(\mathbf{u}) = \int_S \frac{1}{2} |\nabla u^\perp - \nabla v|^2 ds, \quad (3)$$

where  $^\perp$  denotes a counterclockwise  $90^\circ$  rotation in  $S$ . For a 3D surface with normal vector  $\mathbf{n}$ , the counterclockwise rotation of the gradient can be written as:  $\nabla u^\perp = \mathbf{n} \times \nabla u$ .

In order to minimize the energy at a discrete level, we assume the following finite element expansions for  $\mathbf{u} = \{u, v\}$ :

$$\mathbf{u}_h(\mathbf{x}) = \sum_{i \in I} \mathbf{u}_i \phi_i(\mathbf{x}) + \sum_{i \in J} \mathbf{u}_D(\mathbf{x}_i) \phi_i(\mathbf{x}) \quad (4)$$

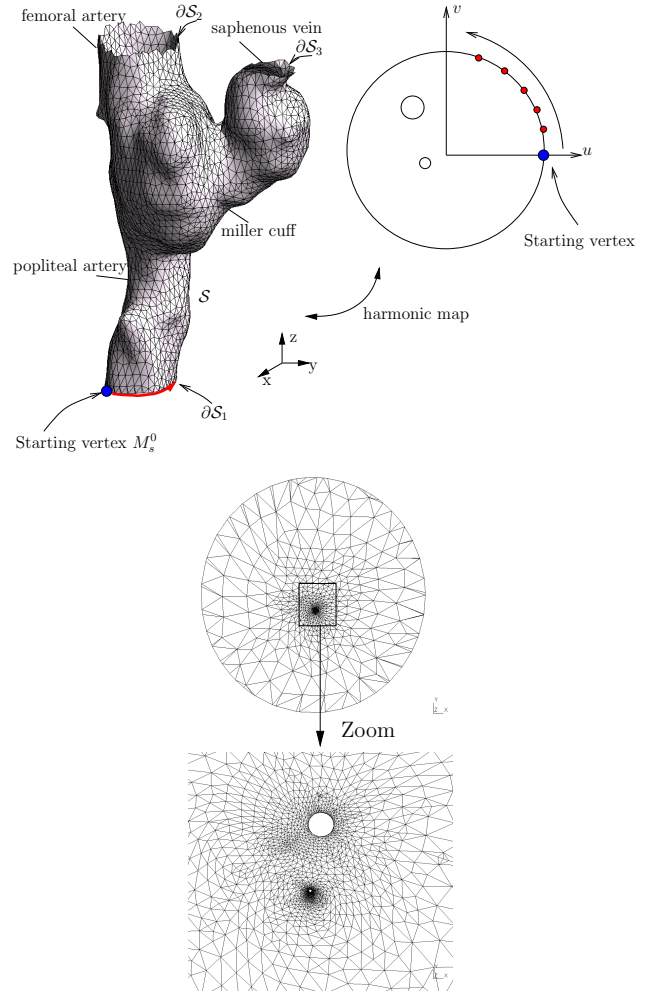


**Figure 1** STL triangulation of an arterial anastomosis and its map onto the unit circle (top) and mapped mesh on the unit circle (bottom). As the geometrical ratio of the initial STL triangulation is higher than 4, the mapped triangles become very small (see zoom) in the parametric unit disk.

where  $I$  denotes the set of nodes of  $S$  that do not belong to the Dirichlet boundary,  $J$  denotes the set of nodes of  $S$  that belong to the Dirichlet boundary and where  $\phi_i$  are the linear nodal shape functions associated with the nodes of the mesh. We assume here that nodal shape function  $\phi_i$  is equal to 1 on vertex  $\mathbf{x}_i$  and 0 on any other vertex:  $\phi_i(\mathbf{x}_j) = \delta_{ij}$ .

The two minimization problems then can then be rewritten as a linear system to solve (see [14, 18]):

$$\underbrace{\begin{pmatrix} \mathbf{A} & -\mathbf{C} \\ -\mathbf{C}^T & \mathbf{A} \end{pmatrix}}_{\mathbf{L}_C} \begin{pmatrix} U \\ V \end{pmatrix} = \begin{pmatrix} \mathbf{0} \\ \mathbf{0} \end{pmatrix}, \quad (5)$$

where  $\mathbf{A}$  is a symmetric positive definite matrix and  $\mathbf{C}$  is an antisymmetric matrix that are both built by assembling the elementary matrices  $A_{kj} = \int_M \nabla \phi_k \cdot \nabla \phi_j ds$  and  $C_{kj} = \int_M \mathbf{n} \cdot (\nabla \phi_k \times \nabla \phi_j) ds$ , and the vectors  $U$  and  $V$  denote respectively the vector of unknowns  $u_k$  and  $v_k$ .

For the harmonic map, we have  $\mathbf{C} = \mathbf{0}$ . The resulting matrix  $\mathbf{L}_C$  is then symmetric definite positive such that the linear system  $\mathbf{L}_C \mathbf{U} = \mathbf{0}$  can be efficiently solved using a direct sparse symmetric-positive-definite solver such as TAUCS<sup>1</sup>.

It is necessary to impose appropriate boundary conditions to guarantee that the discrete minimization problem has a unique solution and that this unique solution defines a one-to-one mapping (and hence avoids the degenerate solution  $\mathbf{u} = \text{constant}$ ). Dirichlet boundary conditions are often used for the Laplacian harmonic map and the convex combination map to map the boundary nodes of  $\partial M_1$  to a unit circle:

$$u_D(\mathbf{x}_i) = \cos\left(\frac{2\pi l_i(\mathbf{x}_i)}{L}\right), \quad v_D(\mathbf{x}_i) = \sin\left(\frac{2\pi l_i(\mathbf{x}_i)}{L}\right). \quad (6)$$

We have decided to map to a unit circle but all kind of convex fixed boundaries could be considered since the mapping is proven to be one-to-one if the mapped surface is convex [3, 16].

Instead of fixing all the boundary nodes  $\partial S_1$  to a convex polygon, one might fix two  $(u, v)$  coordinates, thus pinning down two vertices in the parameter plane with Dirichlet boundary conditions. Indeed, for least square conformal maps, the mapping (5) has full rank only when the number of pinned vertices is greater or equal to 2 [11]. Pinning down two vertices will set the translation, rotation and scale of the solution when solving the linear system  $\mathbf{L}_C \mathbf{U} = \mathbf{0}$  and will lead to what is called a free-boundary parametrization. It was independently found by the authors of the LSCM [11] and the DCP [1] that picking two boundary vertices the farthest from each other seems to give good results in general.

## Volume meshes

We have implemented an advancing layer method [6, 7, 9] for the generation of boundary layers. Those boundary layer meshes are attractive since they present high aspect ratio, orthogonal and possibly graded elements at the wall. The method starts from a surface mesh on which a boundary layer must be grown. From each surface node a direction is picked for placing the nodes of the boundary layer mesh. The direction is either computed using an estimate to the surface normal at the node using Gouraud shading, or specified directly as a three-dimensional vector field—obtained e.g. as the solution of a partial differential equation. The nodes are connected to form layers of prisms that are subsequently subdivided into tetrahedra. This technique is quite efficient in terms of computational time but cannot guarantee that there will not be any overlap at tight corners. Therefore, the user has to take care to produce elements of acceptable shape at sharp corners and to prevent element overlap in regions of tight corners.

These boundary layer meshes can be built by extruding outward and inward the lumen surface. Then a three-

dimensional Delaunay mesh generator is called to fill the remaining of the lumen volume with isotropic tetrahedra. Figure 2 shows an example of volume mesh with boundary layers that is well suited for blood flow simulations in compliant vessels.

It should be noted however that for realistic blood flow simulations, the thickness of the viscous boundary layer mesh and the mesh resolution for the inner tetrahedra are often unknown prior to the computation. An effective approach to overcome this difficulty is to start from the predefined boundary layer meshes as depicted in Fig. 2 and to apply an adaptive procedure [5, 19, 20] where the distribution of the spatial discretization errors are estimated and controlled by modifying the mesh resolution. For example, in the case of unsteady blood flow simulations, one could rely the adaptation of the mesh size field on an Hessian strategy [10] of the average flow speed over one cardiac cycles [19, 20].

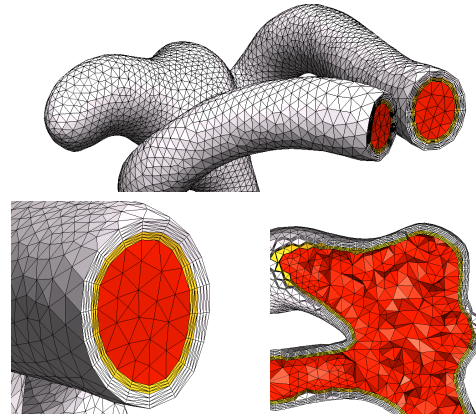


**Figure 2 Magnified views of the boundary layer volume mesh of an aneurysm. The white volume is a boundary layer mesh of the arterial wall, and the red and yellow volumes represent the arterial lumen. The yellow volume is the fluid boundary layer mesh that is built in order to capture accurately the wall shear stresses during the blood flow simulations and the red volume is the remaining of the lumen volume that is filled with isotropic tetrahedra.**

## Results

In this section, we first present two remeshing examples and compare the two different mapping techniques. We compare timings as well as mesh qualities for the new triangulations. The quality of the isotropic meshes is evaluated by computing the aspect ratio of every mesh triangle as follows [8]:

$$\kappa = \alpha \frac{\text{inscribed radius}}{\text{circumscribed radius}} = 4 \frac{\sin \hat{a} \sin \hat{b} \sin \hat{c}}{\sin \hat{a} + \sin \hat{b} + \sin \hat{c}}, \quad (7)$$

$\hat{a}, \hat{b}, \hat{c}$  being the three inner angles of the triangle. With this definition, the equilateral triangle has  $\kappa = 1$  and a flat degenerated triangle has  $\kappa = 0$ .

In the first example, we compare the remeshing of a human aorta with both the harmonic and the conformal map.

<sup>1</sup><http://www.tau.ac.il/~stoledo/taucs/>

As the geometrical aspect ratio of the triangulation is high, the initial mesh has been automatically split by our algorithm into two different mesh patches. The splitting has been performed with our max-cut mesh partitioner based on a multiscale Laplacian map [12]. As can be seen from Fig. 3, the mapped meshes computed with the Laplacian harmonic map present much more distortion close to the boundaries. Again, as most of the planar meshes are more efficient with less distorted meshes, we have that the qualities of the resulting meshes are higher for the conformal map. Indeed, for a radius dependent isotropic remeshing of the aorta, we obtain a minimum quality of  $\kappa_{min} = 0.04$  for the harmonic map and  $\kappa_{min} = 0.39$  for the conformal map. The mean quality is  $\bar{\kappa} = 0.91$  for the harmonic map and  $\bar{\kappa} = 0.96$  for the conformal map. Here, a Frontal planar mesher was chosen for the remeshing in the parametric space. The initial triangulation of the aorta contains 12000 triangles and the remeshing procedure for a new mesh of 5500 triangles took us less than 4s.

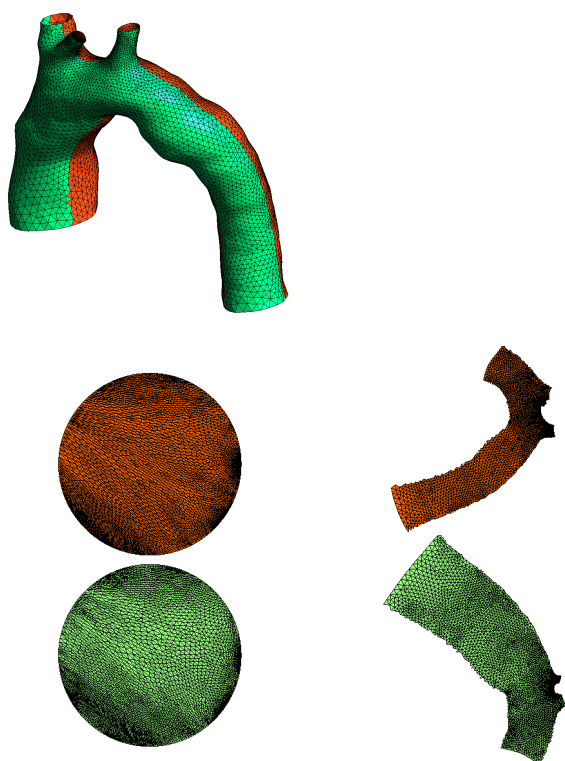


**Figure 3** Remeshing of an STL triangulation of a human aorta that has been split into two mesh patches (top). Harmonic mapping (bottom left) and conformal mapping (bottom right) for those two patches.

We further illustrate the capabilities of our algorithm by showing the remeshing of airways models presented in Figs.4 and 5. The presented algorithm is compared with the meshing algorithm of Mimics. Mimics uses a two step mesh adaptation strategy in order to optimize the initial STL triangulation: in a first step three iterations of remeshing improve skewness to a minimal value of 0.4.

In this step the maximal edge length is set to  $0.5\text{ mm}$  and the maximal geometrical error to  $0.01\text{ mm}$ . Hereafter a quality preserving triangle reduction is performed. Again three iterations are done with a maximal edge length set to  $0.5\text{ mm}$  and the maximal geometrical error set to  $0.05\text{ mm}$ . This provides the final remeshed model with Mimics. In comparison, our technique relies on a multiscale partitioning of the airway models into two parts of moderate geometrical aspect ratio. Each of those two parts is then parametrized using a harmonic map and the remeshing is then performed in the parametric plane using standard 2D meshing algorithms (MeshAdapt, Delaunay or frontal). As can be seen in Figs.4 and 5, the quality of the meshes obtained with a remeshing procedure based on a harmonic map is much higher than with the mesh adaptation strategies (such as the one implemented in Mimics).

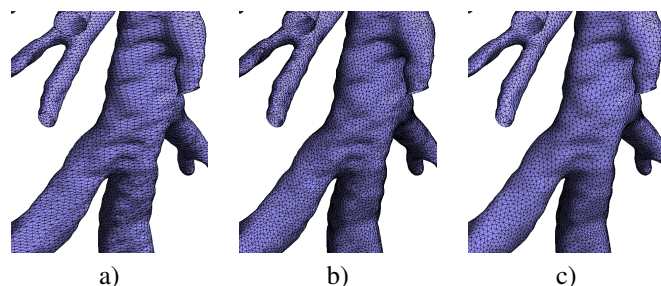


**Figure 4** Remeshing of human lungs: a) part of the initial STL triangulation, b) remeshed geometry with Mimics (after 2 steps) and c) remeshed lung based on the Harmonic mapping remeshing procedure.

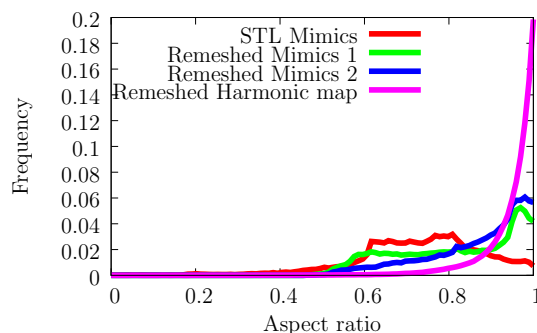


**Figure 5** Remeshing of human lungs with the presented algorithm as compared with a commercial package such as Mimics.

The next example studies the flow in a simplified aortic arch. The STL triangulation was found on the INRIA web site<sup>2</sup>. The STL surface mesh has been remeshed using the presented techniques based on conformal maps. The initial STL has a mean quality of  $\bar{\kappa} = 0.39$ , while the new surface mesh has  $\bar{\kappa} = 0.94$ . Accurate and converged numerical simulations are mandatory since it has been shown that the flow patterns and the locations of low wall shear

<sup>2</sup><http://www-c.inria.fr/Eric.Saltel/saltel.php>

stress (WSS) correspond with locations of aneurysm formation in the descending aorta [15, 22]. The wall shear stress is defined as the norm of the shear stress at the wall:

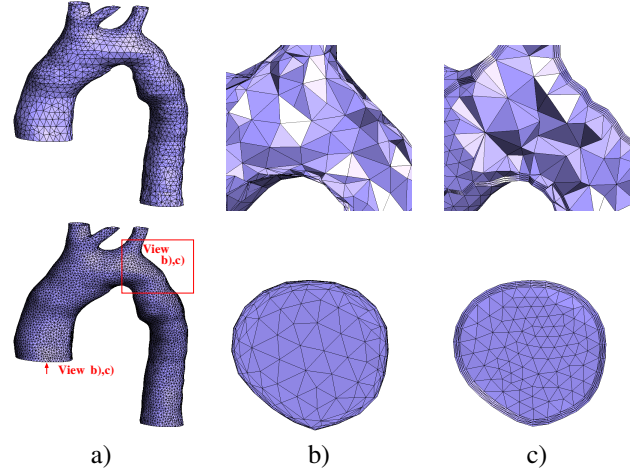
$$WSS = \|\vec{t}_w\| = \|\vec{t} - (\vec{t} \cdot \vec{n}) \cdot \vec{n}\|, \quad (8)$$

with  $\vec{t} = \mu (\nabla \vec{u} + \nabla \vec{u}^T) \cdot \vec{n}$ .

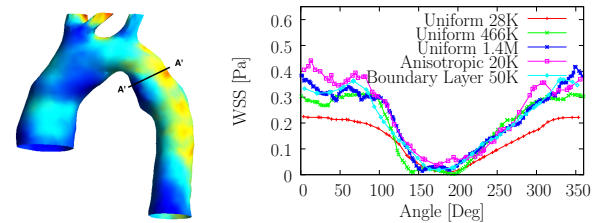
For the numerical simulation, we apply simple boundary conditions: a parabolic velocity profile at the inlet (heart) and zero natural pressure boundary conditions at the outlets (innominate artery, left common carotid artery, left subclavian artery and descending aorta) and a zero velocity (no-slip) on the vessel walls. We consider a stationary flow at Reynolds  $Re = 450$  and different meshes: isotropic volume meshes of respectively  $28K$ ,  $160K$  and  $466K$  tetrahedra and an adapted anisotropic mesh that has approximately  $20K$ . We first compute an isotropic surface mesh with our remeshing algorithm and then produce two different types of volume meshes: (i) isotropic volume meshes of different prescribed mesh sizes, (ii) adapted anisotropic volume meshes and (ii) a boundary layer mesh obtained by extrusion of the surface mesh over a number of layers (5 layers in the boundary  $\delta_{bl} = 1/\sqrt{Re}$ ). Adaptive refinement in the boundary with either anisotropic metric fields or boundary layers is indeed attractive [2, 19, 21] to increase the solution accuracy in the region of interest (at the wall) and this way decrease the load on the solver by reducing the number of finite elements used. With the presented approach of harmonic map, we do have a parametric description of the initial triangulation that enables us to use anisotropic mesh adaptation libraries such as our open source MadLib library [4]. This library aims at modifying the initial mesh to make it comply with criteria on edge lengths and element shapes by applying a set of standard mesh modifications (edge splits, edge collapses and edge swaps, etc.). An anisotropic field based on the distance to the wall and the curvature can then be defined in order to generate boundary layer meshes. In the example presented in Fig.6c), we prescribe a small size with a linear growth in the normal direction to the wall, and three times a larger size is prescribed in the tangent directions. The final mesh metric field is built from those resulting sizes and directions. It should be noted that a volume mesh was also produced from the STL triangulation but this volume mesh was of too low quality to obtain a convergence of the numerical simulation ( $\gamma_{min} = 1.5e^{-5}$  and  $\bar{\gamma} = 0.45$ ).

Figure 6 shows the initial STL triangulation, a remeshed isotropic surface mesh, and a mesh cut of the volume anisotropic mesh. As can be seen, initial STL triangulation is faceted and the horizontal structure of the CT slices are visible.

Figure 7 shows the WSS values computed for different meshes at section  $A - A'$ . We selected section  $A - A'$  since this section intersects the regions of low and high WSS. For this section, the WSS values vary in the azimuthal direction, the zero angle corresponding to the location  $A'$ . As can be seen in Fig.7, the high quality isotropic volume meshes converge well towards an azimuthal WSS



**Figure 6 Aortic arch meshes: a) Initial STL triangulation (top) and remeshed surface (isotropic mesh size), b) Anisotropic volume mesh cut created from the remeshed surface with MADLib, c) Boundary layer volume mesh.**



**Figure 7 Blood flow simulation in an aortic arch. The left figure shows the WSS distribution and the right figure the WSS along the circumference at section  $A - A'$  for different meshes for a constant inlet flow rate. The zero angle corresponds to the location  $A'$ .**

distribution. The WSS for the anisotropic mesh exhibits more numerical noise that is due to the velocity gradient computations involved in (8) that are less accurate for highly anisotropic meshes [2, 19, 21]. Meanwhile, the mean values (max and min WSS) converge towards the one obtained with the finest isotropic mesh within a smaller computational time (mesh of only  $20K$ ). The boundary layer volume mesh provides less oscillatory results and show also convergence towards the finest isotropic mesh for a reduced number of elements ( $50K$  versus  $1.4M$  tetrahedra).

## Conclusions

In this work, we have presented a fully automatic open source approach to recover a high quality surface and volume mesh from low-quality oversampled inputs (STL files) obtained via 3D acquisition systems. The approach is original as it combines an efficient and robust parametrization technique based on harmonic maps [17]. With the present approach, we are able to remesh any surface with any topological genus and with large geometrical aspect ratio such as arteries. We showed that the remeshing procedure is

highly efficient and produces high-quality meshes that are suitable for finite element biological flow simulations.

## References

- [1] P. Alliez, M. Meyer, and M. Desbrun. Interactive geometry remeshing. *Computer graphics (Proceedings of the SIGGRAPH 02)*, pages 347–354, 2002.
- [2] L. Botti, M. Piccinelli, B. Ene-Iordache, A. Remuzzi, and L. Antiga. An adaptive mesh refinement solver for large-scale simulation of biological flows. *Communications in Numerical Methods in Engineering*, 2009.
- [3] C. Choquet. Sur un type de représentation analytique généralisant la représentation conforme et définie au moyen de fonctions harmoniques. *Bull. Sci. Math*, 69(156-165), 1945.
- [4] G. Compère and J.-F. Remacle. Website of madlib: Mesh adaptation library, 2008. <http://www.madlib.be>.
- [5] G. Compère and J.-F. Remacle. A mesh adaptation framework for large deformations. *International Journal for Numerical Methods in Engineering*, 82(7):843–867, 2009.
- [6] S. Connell and M. Braaten. Semistructured mesh generation for three-dimensional navier-stokes calculations. *AIAA Journal*, 33(6):1017–1024, 1995.
- [7] R. V. Garimella and M. S. Shephard. Boundary layer mesh generation for viscous flow simulations. *International Journal for Numerical Methods in Engineering*, 49(1):193–218, 2000.
- [8] C. Geuzaine and J.-F. Remacle. Gmsh: a three-dimensional finite element mesh generator with built-in pre- and post-processing facilities. *International Journal for Numerical Methods in Engineering*, 79(11):1309–1331, 2009.
- [9] Y. Kallinderis, A. Khawaja, and H. McMorris. Hybrid prismatic/tetrahedral grid generation for complex geometries. *AIAA Paper*, 34:93–0669, 1996.
- [10] G. Kunert. Anisotropic mesh construction and error estimation in the finite element method. *Numer. Methods Partial Differential Equations*, 18:625–648, 2000.
- [11] B. Levy, S. Petitjean, N. Ray, and J. Maillot. Least squares conformal maps for automatic texture atlas generation. In *Computer Graphics (Proceedings of SIGGRAPH 02)*, pages 362 – 371, 2002.
- [12] E. Marchandise, C. Carton de Wiart, W. Vos, C. Geuzaine, and J.-F. Remacle. High quality surface remeshing using harmonic maps. Part II: Surfaces with high genus and of large aspect ratio. *International Journal for Numerical Methods in Engineering*, online 2011.
- [13] E. Marchandise, G. Compère, M. Willemet, G. Bricteux, C. Geuzaine, and J.-F. Remacle. Quality meshing based on stl triangulations for biomedical simulations. *International Journal for Numerical Methods in Biomedical Engineering*, 83:876–889, 2010.
- [14] E. Marchandise, P. Crosetto, C. Geuzaine, J.-F. Remacle, and E. Sauvage. *Quality open source mesh generation for cardiovascular flow simulations*, volume accepted of *Springer Series on Modeling, Simulation and Applications*, chapter of modelling physiological flows. Springer-Verlag, Berlin Heidelberg, 2011.
- [15] K. D. O’Brien and A. Chait. The biology of the artery wall in atherogenesis. *The Medical clinics of North America*, 78(1):41–67, 1994.
- [16] T. Rado. Aufgabe 41. *Math-Verien*, page 49, 1926.
- [17] J.-F. Remacle, C. Geuzaine, G. Compère, and E. Marchandise. High quality surface remeshing using harmonic maps. *International Journal for Numerical Methods in Engineering*, 83(403-425), 2010.
- [18] J.-F. Remacle, J. Lambrechts, B. Seny, and E. Marchandise. Blossom-quad: a non-uniform quadrilateral mesh generator using a minimum cost perfect matching algorithm. *International Journal for Numerical Methods in Engineering*, submitted 2011.
- [19] O. Sahni, K. Jansen, and M. Shephard. Automated adaptive cardiovascular flow simulations. *Engineering with Computers*, 25(1):25–36, 2009.
- [20] O. Sahni, K. E. Jansen, M. S. Shephard, C. A. Taylor, and M. W. Beall. Adaptive boundary layer meshing for viscous flow simulations. *Eng. with Comput.*, 24(3):267–285, 2008.
- [21] O. Sahni, J. Mueller, K. Jansen, M. Shephard, and C. Taylor. Efficient anisotropic adaptive discretization of cardiovascular system. *Comp. Meth. Appl. Mech. Eng.*, 195:5634–5655, 2006.
- [22] A. M. Shaaban and A. Duerinckx. Wall shear stress and early atherosclerosis. *American Journal of Roentgenology*, 174:1657–1665, 2000.